Trk receptor signaling and sensory neuron fate are perturbed in human neuropathy caused by *Gars* mutations

James N. Sleigh[a,1], John M. Dawes[b,2], Steven J. West[b,2], Na Wei[c], Emily L. Spaulding[d,e], Adriana Gómez-Martín[a], Qian Zhang[c], Robert W. Burgess[d,e], M. Zameel Cader[b], Kevin Talbot[b], Xiang-Lei Yang[c], David L. Bennett[b], and Giampietro Schiavo[a,1]

[a]Sobell Department of Motor Neuroscience and Movement Disorders, Institute of Neurology, University College London, London WC1N 3BG, United Kingdom; [b]Nuffield Department of Clinical Neurosciences, University of Oxford, John Radcliffe Hospital, Oxford OX3 9DU, United Kingdom; [c]Department of Molecular Medicine, The Scripps Research Institute, La Jolla, CA 92037; [d]The Jackson Laboratory, Bar Harbor, ME 04609; and [e]Graduate School of Biomedical Science and Engineering, University of Maine, Orono, ME 04469

Edited by Clifford J. Woolf, Children's Hospital Boston and Harvard Medical School, Boston, MA, and accepted by Editorial Board Member Pietro De Camilli March 6, 2017 (received for review August 31, 2016)

Charcot–Marie–Tooth disease type 2D (CMT2D) is a peripheral nerve disorder caused by dominant, toxic, gain-of-function mutations in the widely expressed, housekeeping gene, *GARS*. The mechanisms underlying selective nerve pathology in CMT2D remain unresolved, as does the cause of the mild-to-moderate sensory involvement that distinguishes CMT2D from the allelic disorder distal spinal muscular atrophy type V. To elucidate the mechanism responsible for the underlying afferent nerve pathology, we examined the sensory nervous system of CMT2D mice. We show that the equilibrium between functional subtypes of sensory neuron in dorsal root ganglia is distorted by *Gars* mutations, leading to sensory defects in peripheral tissues and correlating with overall disease severity. CMT2D mice display changes in sensory behavior concordant with the afferent imbalance, which is present at birth and nonprogressive, indicating that sensory neuron identity is prenatally perturbed and that a critical developmental insult is key to the afferent pathology. Through in vitro experiments, mutant, but not wild-type, GlyRS was shown to aberrantly interact with the Trk receptors and cause misactivation of Trk signaling, which is essential for sensory neuron differentiation and development. Together, this work suggests that both neurodevelopmental and neurodegenerative mechanisms contribute to CMT2D pathogenesis, and thus has profound implications for the timing of future therapeutic treatments.

aminoacyl-tRNA synthetase | Charcot–Marie–Tooth disease | distal spinal muscular atrophy type V | neuromuscular disease | neurodevelopment

Charcot–Marie–Tooth disease (CMT) is a group of genetically diverse peripheral neuropathies that share the main pathological feature of progressive motor and sensory degeneration (1). Although lifespan is usually unaffected, patients display characteristic muscle weakness and wasting predominantly in the extremities, leading to difficulty walking, foot deformities, and reduced dexterity (2). CMT is traditionally divided into type 1/demyelinating CMTs that display loss of peripheral nerve myelin causing reduced nerve conduction velocity (NCV), type 2/axonal CMTs typified by axon loss with relatively normal NCVs, and intermediate CMTs that share clinical features of CMT1 and -2 (1). Over 80 different genetic loci have been linked to CMT, which is known to affect ∼1/2,500 people, making it the most common group of hereditary neuromuscular disorders (3).

Dominant mutations in the glycyl-tRNA synthetase (GlyRS) gene, *GARS*, are causative of CMT type 2D (CMT2D) [Online Mendelian Inheritance in Man (OMIM) 601472], which normally manifests during adolescence and presents with muscle weakness in the extremities (4). The 2D subtype is one of a number of CMTs associated with mutation of an aminoacyl-tRNA synthetase (ARS) gene (5–8). Humans possess 37 ARS proteins, which covalently link amino acids to their partner transfer RNAs (tRNAs), thereby charging and priming the tRNAs for protein synthesis. This housekeeping function of glycine aminoacylation explains the widespread and constitutive nature of *GARS* expression (4), but at the same time stresses the phenomenon of neuronal specificity in the disease: Why do mutations that affect a ubiquitous protein selectively trigger peripheral nerve degeneration? Several hypotheses have been suggested (9, 10), although the exact disease mechanisms remain unknown. Nevertheless, cell-based experiments and studies using two CMT2D mouse models (the mild $Gars^{C201R/+}$ allele and the more severe $Gars^{Nmf249/+}$ strain) indicate that CMT2D is likely caused by a toxic gain of function in mutant GlyRS rather than haploinsufficiency due to a loss of aminoacylation activity or a noncanonical function (11–15). A possible mediator of toxicity was identified when five CMT2D-associated mutations spread along the length of *GARS* were all shown to induce a similar conformational change in GlyRS, leading to the exposure of surfaces buried in the wild-type protein (16). These neomorphic regions likely facilitate the aberrant accumulation of mutant GlyRS at the neuromuscular junction (NMJ) of a CMT2D *Drosophila melanogaster* model (17), and nonphysiological extracellular interaction of mutant GlyRS with

Significance

The mechanisms triggering motor and sensory nerve dysfunction in the genetically diverse Charcot–Marie–Tooth disease (CMT) remain unresolved, as does the reason for the lack of sensory pathology observed in distal hereditary motor neuropathies, which can be associated with CMT genes. To unravel the pathways leading to afferent deterioration, we have studied the sensory nervous system of CMT type 2D (CMT2D) mice. Our work demonstrates that the specific cellular identity of sensory nerves is perturbed in mutant mice prenatally, and that this is likely caused by aberrant interaction of mutant CMT2D protein with Trk receptors impacting their prodifferentiation/development signaling. CMT therefore manifests through malfunctioning of the complex interplay between developmental, maturation, and survival programs, which has important implications for therapeutic timing.

Author contributions: J.N.S., J.M.D., S.J.W., N.W., X.-L.Y., D.L.B., and G.S. designed research; J.N.S., J.M.D., S.J.W., N.W., E.L.S., A.G.-M., and Q.Z. performed research; J.N.S., J.M.D., and S.J.W. analyzed data; and J.N.S., J.M.D., S.J.W., N.W., R.W.B., M.Z.C., K.T., X.-L.Y., D.L.B., and G.S. wrote the paper.

The authors declare no conflict of interest.

This article is a PNAS Direct Submission. C.J.W. is a Guest Editor invited by the Editorial Board.

Freely available online through the PNAS open access option.

[1]To whom correspondence may be addressed. Email: j.sleigh@ucl.ac.uk or giampietro.schiavo@ucl.ac.uk.

[2]J.M.D. and S.J.W. contributed equally to this work.

This article contains supporting information online at www.pnas.org/lookup/suppl/doi:10.1073/pnas.1614557114/-/DCSupplemental.

www.pnas.org/cgi/doi/10.1073/pnas.1614557114

neuropilin 1 (NRP1), which antagonizes VEGF signaling (18). This aberrant binding and noncell autonomous toxicity is contingent upon GlyRS secretion, which occurs from a number of different cell types in culture and is unaffected by neuropathy-associated mutations (17–19).

A second major conundrum in GlyRS-associated neuropathy is why some patients with dominant *GARS* mutations and diagnosed with the allelic neuropathy distal spinal muscular atrophy type V (dSMA-V, OMIM 600794) (4), lack the distinguishing mild-to-moderate sensory involvement typical of CMT2D (20–23). The ability of patients with CMT2D to sense vibration is most impaired, followed by light touch, temperature, and pain (20). Furthermore, patients with CMT2D display deficits in deep tendon reflexes of the extremities (22, 23), whereas reflexes of patients with dSMA-V remain relatively unperturbed (4, 24), implicating defective relay arc afferents rather than efferents. CMT2D sensory defects are dependent on disease severity, but not duration, whereas patients with dSMA-V are refractory to sensory pathogenesis, suggesting that, similar to other neurological diseases (25), the two disorders lie along a spectrum and that disease-modifying loci may dictate these differences (20). Accordingly, CMT2D and dSMA-V can be caused by the same *GARS* mutation and manifest at different ages within a family (21).

CMT2D sensory pathology, both in patients and animal models, has not been studied in detail, although the limited sensory data currently available have highlighted possible contradictions that require clarification. The greatest sensory deficiency in patients with CMT2D is in the perception of vibration, which is sensed by neurons with large cell bodies and axons (26, 27); however, patient sural nerve biopsies show a selective loss of small sensory axons (20, 21). This histological finding is also counter to what is observed in CMT2D mice; the milder $Gars^{C201R/+}$ mice display a general reduction in axon diameter in both the saphenous and sensory femoral nerves (12), whereas the more severe $Gars^{Nmf249/+}$ allele displays both a reduction in axon diameter and axon number (11); nevertheless, whether specific sensory neuron populations are preferentially atrophied or lost is unknown. We thus set out to interrogate the sensory nervous system of CMT2D mice to better understand how and when *Gars* mutations cause sensory pathology, its molecular mechanism, and the effect that these mutations have on sensation of the external environment.

Results

$Gars^{C201R/+}$ Dorsal Root Ganglion Cultures Have a Smaller Percentage of Large Area Sensory Neurons. We began our CMT2D sensory analysis by culturing primary dorsal root ganglion (DRG) neurons from wild-type and $Gars^{C201R/+}$ mice. This model of CMT2D has a mutagen-induced T456C alteration in the endogenous mouse *Gars* gene, causing a cysteine-to-arginine switch at residue 201; this produces a range of peripheral nerve defects without affecting survival, reminiscent of CMT2D (12). DRG are heterogeneous collections of neural crest-derived sensory neuron cell bodies found in pairs at each segment of the spinal cord, from where they project to and receive information from target peripheral tissues. We chose the time point of 1 mo, because the $Gars^{C201R/+}$ mice are beginning to show overt symptoms, and we have previously performed detailed analyses of their neuromuscular synapses at this age (28).

Thoracic and lumbar DRG neurons were cultured from wild-type and mutant mice, fixed 24 h later, and stained with the panneuronal marker βIII-tubulin to highlight afferent nerve cell somas and processes. Mutant cultures showed no difference from wild type in the percentage of cells bearing neurites (Fig. 1*A*, *Top Left*) or the length of the longest neurite (Fig. 1*A*, *Top Right*); however, there was a significant reduction in the cell body area of $Gars^{C201R/+}$ neurons (Fig. 1*A*, *Bottom Left*). Cultures were also costained with the apoptotic marker-activated caspase 3, and average fluorescence intensity per neuron was measured at 4, 48, and 96 h postplating (Fig. 1*A*, *Bottom Right*). There was no difference between genotypes, suggesting that mutant neurons are as healthy as wild type up to 4 d in culture, and that cell death in vitro is unlikely to be a major contributing factor to the diminished soma area phenotype.

Sensory neurons can be broadly divided into functional classes based on their stimulus response; for example, mechanosensitive neurons that respond to touch, proprioceptive neurons that sense body position in space, and nociceptors that relay noxious stimuli. These classes have been linked to a range of anatomical and physiological characteristics, such as cell soma size, presence of cell-specific protein markers, and electrophysiological properties, which can be used for reliable functional identification (26, 29). Disparate sensory subtype sensitivities have previously been observed in mouse models of peripheral nerve disease (30, 31). To see whether a particular kind of sensory neuron may be preferentially affected by the *Gars C201R* mutation, we divided the βIII-tubulin$^+$ cell bodies into small, medium, and large area neurons based on previously suggested criteria (32). Within these size groups, we again saw no difference between neurite length or cell death levels of wild-type and mutant neurons (*SI Appendix*, Fig. S1). However, we did observe a significantly smaller percentage of large area neurons in $Gars^{C201R/+}$ cultures (Fig. 1*B*). This result confirms the smaller average mutant cell body area and begins to clarify the etiology of the phenotype, as it could be due to an increase in small area neurons without large soma neurons being affected.

To differentiate between large and small sensory neurons at the molecular level, and thereby rule out the smaller body size of mutant mice as being the cause of the reduced cell soma area,

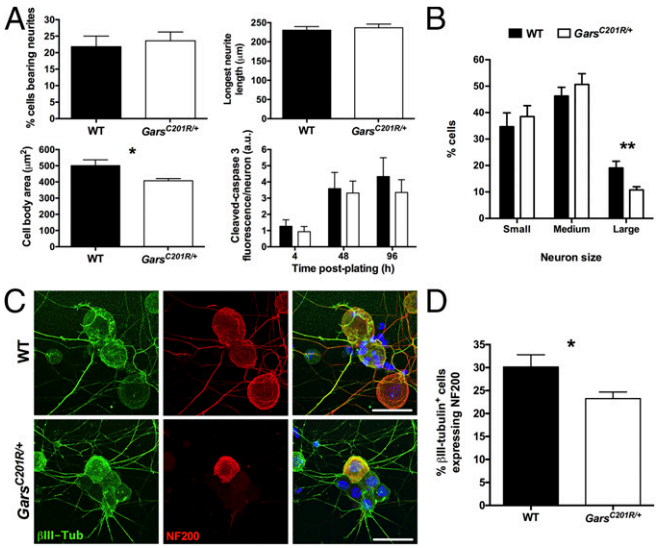

Fig. 1. $Gars^{C201R/+}$ primary DRG cultures have a smaller percentage of large area/NF200$^+$ sensory neurons. (*A*) $Gars^{C201R/+}$ sensory neurons show no difference in the percentage of cells bearing neurites (*Top Left*, $P = 0.678$, unpaired *t* test) or the longest neurite length (*Top Right*, $P = 0.647$, unpaired *t* test), but have a significantly smaller cell body area (*Bottom Left*, $*P = 0.022$, unpaired *t* test). Moreover, mutant cultures do not show signs of cell death above wild-type levels, as assessed by cleaved-caspase 3 staining intensity per neuron (*Bottom Right*, two-way ANOVA, $P = 0.002$, time point; $P = 0.421$, genotype; $P = 0.885$, interaction between the two variables). a.u., arbitrary units. (*B*) Mutant DRG cultures possess a significantly lower percentage of large area neurons (cell body area >706 μm^2, see *SI Appendix, SI Materials and Methods* for criteria) than wild type. $**P = 0.008$, unpaired *t* test between percentage of large cells. (*C*) Representative collapsed z-stack images of wild-type (*Top*) and $Gars^{C201R/+}$ (*Bottom*) DRG neurons stained for the panneuronal marker βIII-tubulin (green), the medium–large neuron marker neurofilament 200 (NF200, red), and DAPI (blue). (Scale bars, 20 μm.) (*D*) Consistent with the reduced percentage of large area neurons (*B*), $Gars^{C201R/+}$ cultures have a lower percentage of cells expressing NF200. $*P = 0.013$, Mann–Whitney *u* test. $n = 4$ (*A* and *B*) and $n = 6$ (*D*). See also *SI Appendix*, Figs. S1 and S2*A*.

antineurofilament 200 (NF200) was used to mark medium–large neurons with myelinated axons (*SI Appendix*, Fig. S2*A*), often described as A fibers (33). Corroborating the cell body measurements, $Gars^{C201R/+}$ cultures had a significantly smaller percentage of βIII-tubulin$^+$ cells (green) that expressed NF200 (red) than wild type (Fig. 1 *C* and *D*). We have thus confirmed at both the morphological and biochemical levels that mutant *Gars* DRG cultures display a significantly reduced percentage of large area neurons.

Sensory, but Not Motor, Identity Is Perturbed in Vivo. To resolve whether the in vitro sensory phenotypes are present in vivo, lumbar DRG were dissected from 1-mo-old animals and sectioned, and immunohistochemical analysis was performed using established markers. Staining for βIII-tubulin (green, Fig. 2*A*), the in vitro phenotype of significantly reduced soma size in $Gars^{C201R/+}$ DRG was replicated in vivo (Fig. 2*B*). In addition to NF200, peripherin expression demarcates cell somas of small diameter neurons with thinly myelinated or unmyelinated axons (Aδ and C fibers, *SI Appendix*, Fig. S2*A*) (34), with the two markers being largely mutually exclusive (35). There is some contention as to whether NF200 and peripherin are good indicators of myelination (36); nevertheless, they are well-established neuronal size indicators. Anti-NF200 and anti-peripherin were thus used to identify medium–large (red) and small (green) sensory neurons, respectively (Fig. 2*C* and *SI Appendix*, Fig. S2*B*). $Gars^{C201R/+}$ DRG show a significantly smaller percentage of NF200-expressing cells (Fig. 2*D*) and a reciprocal increase in the percentage of peripherin$^+$ cells (Fig. 2*E*). There was only a small degree of coexpression between the two markers (2.3 ± 0.3% versus 2.5 ± 0.4%). The percentage of NF200-expressing wild-type cells is similar to that previously reported (37). Corroborating this result, NF200 and peripherin protein levels were shown to be reduced and increased, respectively, in 1-mo lumbar DRG lysates from $Gars^{C201R/+}$ mice (Fig. 2 *F* and *G*). We have thus shown that the in vitro $Gars^{C201R/+}$ sensory phenotype of having a smaller percentage of large area/NF200$^+$ cells is confirmed in vivo.

To determine whether NF200-expressing cells are selectively affected, DRG sections were tested for the presence of activated caspase 3 (green, *SI Appendix*, Fig. S3 *A–C*). Similar to the in vitro results, mutant DRG sections showed no increase in cleaved-caspase 3 signal (*SI Appendix*, Fig. S3*B*), indicating that postnatal cell death is unlikely to be playing a critical role in the reduced percentage of NF200$^+$ cells. To test whether mutant ganglia contain increased numbers of peripherin-expressing cells, serial sectioning of L5 DRG was performed (*SI Appendix*, Fig. S3*D*). L5 was chosen due to its size and because the resident sensory neurons target distal tissues of the hind limbs, where neuromuscular pathology occurs in *Gars* mice (11, 15, 28). Counting βIII-tubulin$^+$ (red) cell profiles to estimate the number of neurons per DRG, we found no difference between wild-type and mutant ganglia (*SI Appendix*, Fig. S3*E*). These profile counts are similar to published approximations from both mice and rats (38, 39). Given the lack of cell death and similar cell profile

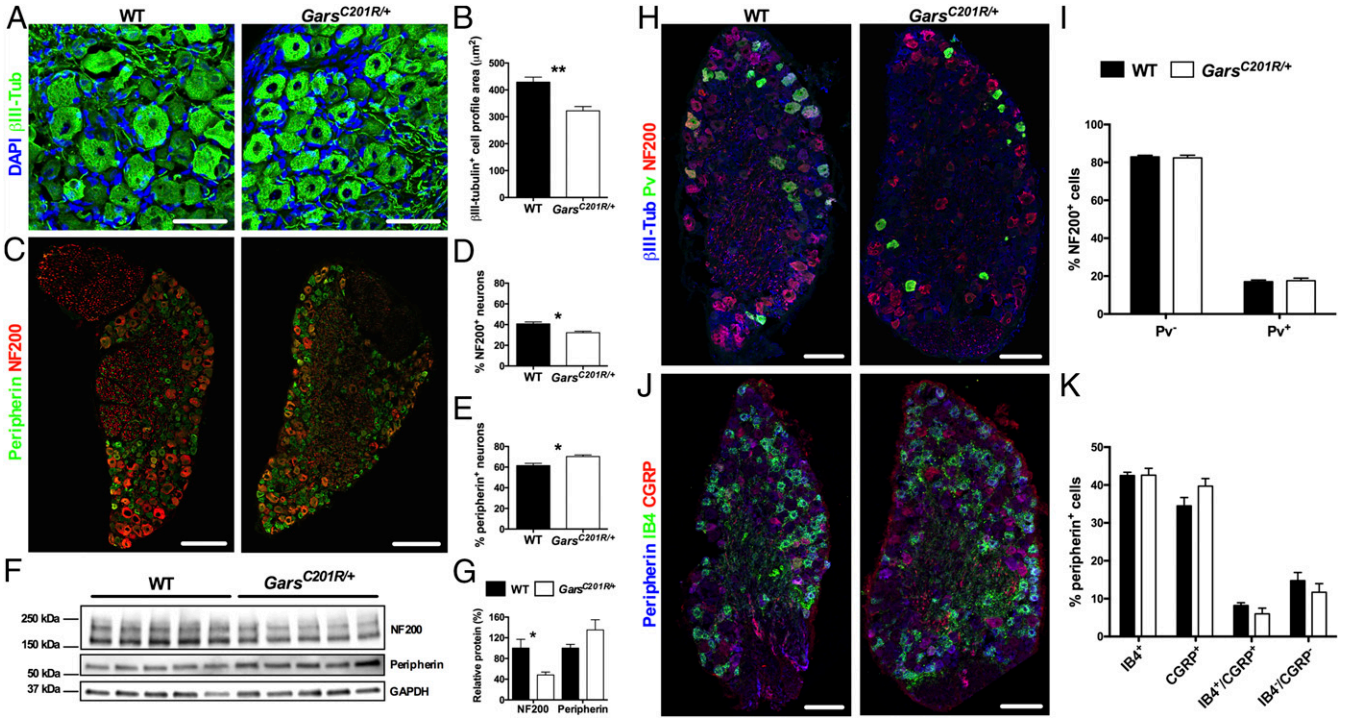

Fig. 2. Mutant DRG have a smaller percentage of large area sensory neurons at 1 mo in vivo. (*A*) Representative collapsed z-stack images of wild-type (*Left*) and $Gars^{C201R/+}$ DRG at 1 mo stained for DAPI (blue) and the panneuronal marker βIII-tubulin (green). (*B*) The average cell profile area of mutant sensory neurons is significantly smaller than wild type. $^{**}P = 0.005$, unpaired *t* test. (*C*) Representative wild-type and $Gars^{C201R/+}$ DRG stained for NF200 (red), marking medium–large sensory neurons, and peripherin (green), labeling small sensory neurons. (*D* and *E*) Compared with wild type, mutant DRG possess a significantly smaller percentage of NF200$^+$ cells (*D*, $^*P = 0.011$, unpaired *t* test) and a concomitant increase in the percentage of peripherin$^+$ cells (*E*, $^*P = 0.015$, unpaired *t* test). (*F* and *G*) Representative Western blot of 1-mo lumbar DRG protein lysates and densitometry analysis confirming the reduced NF200 ($^*P = 0.020$, unpaired *t* test) and increased peripherin ($P = 0.131$, unpaired *t* test) levels in mutant ganglia. (*H*) Representative 1-mo wild-type and $Gars^{C201R/+}$ DRG sections stained to identify mechanoreceptive (NF200$^+$ [red]/Pv$^-$) and proprioceptive neurons (*A*, NF200$^+$/Pv$^+$[green]). (*I*) $Gars^{C201R/+}$ DRG show no difference in the percentage of NF200$^+$ cells that costain for the proprioceptive marker parvalbumin (Pv). $P = 0.768$, unpaired *t* test between Pv$^-$ cells. (*J*) Representative images of wild-type and $Gars^{C201R/+}$ DRG at 1 mo stained to identify nonpeptidergic nociceptors (peripherin$^+$[blue]/IB4$^+$[green]/CGRP$^-$), and peptidergic nociceptors (peripherin$^+$/IB4$^-$/CGRP$^+$[red]). (*K*) There is also no difference between the percentages of wild-type and mutant peripherin$^+$ sensory neurons expressing either IB4 or CGRP. $P = 0.964$ and $P = 0.132$, unpaired *t* test between IB4$^+$ cells and CGRP$^+$ cells, respectively. $n = 4–5$. Images in *C*, *H*, and *J* are single confocal planes. [Scale bars, 50 μm (*A*) and 100 μm (*C*, *H*, and *J*).] See also *SI Appendix*, Figs. S1–S5.

counts, the alteration of sensory subtypes in $Gars^{C201R/+}$ DRG at 1 mo in vivo are consistent with a perturbation of neuronal fate.

As CMT2D affects both the sensory and motor systems, we stained lumbar spinal cord sections from 1 mo wild-type and $Gars^{C201R/+}$ mice to determine whether α- and γ-motor neurons are also disturbed. $Gars^{C201R/+}$ mice do not show loss of motor neuron cell bodies up to at least 4 mo in the lumbar spinal cord (12). α-Motor neurons innervate force-generating extrafusal muscle fibers, whereas the smaller γ-motor nerves innervate intrafusal fibers of muscle spindles (40). The presence of NeuN distinguishes between α- and γ-motor neurons (*SI Appendix*, Fig. S4*A*); cells found in spinal cord lamina IX expressing both choline acetyltransferase (ChAT) and NeuN are α-motor neurons, whereas $ChAT^{+}/NeuN^{-}$ cells are γ-motor neurons (*SI Appendix*, Fig. S4*B*) (41). No difference between α- and γ-motor neurons proportions were observed (*SI Appendix*, Fig. S4*C*), indicating that sensory neuron identity is specifically disturbed by *Gars* mutation.

The Alteration in Sensory Neuron Subtypes Correlates with Overall Disease Burden in CMT2D Mice. We have previously shown that NMJ pathology correlates with CMT2D severity by comparing $Gars^{C201R/+}$ with the more severe $Gars^{Nmf249/+}$ mouse mutant (28, 42), which displays frank denervation, peripheral axon loss, and genetic background-dependent mortality at 6–8 wk (11). This model has a spontaneous CC-to-AAATA mutation, causing proline at residue 278 to be substituted for lysine and tyrosine (11). Similar to the milder allele, 1-mo-old $Gars^{Nmf249/+}$ DRG possessed a significantly lower percentage of $NF200^{+}$ (red) somas (*SI Appendix*, Fig. S5 *A* and *B*) and a significantly greater percentage of $peripherin^{+}$ (green) neurons compared with wild type (*SI Appendix*, Fig. S5 *A* and *C*). When the values from both mutant alleles were compared, $Gars^{Nmf249/+}$ DRG had a significantly lower percentage of NF200-expressing cells than $Gars^{C201R/+}$ (*SI Appendix*, Fig. S5*B*) and a significantly higher percentage of $peripherin^{+}$ cells (*SI Appendix*, Fig. S5*C*). Importantly, the results hold true when $Gars^{C201R/+}$ and $Gars^{Nmf249/+}$ mutant percentage values relative to their respective wild types are statistically compared for both NF200 ($Gars^{C201R/+}$, 79.1 ± 3.4% versus $Gars^{Nmf249/+}$, 56.6 ± 7.4%) and peripherin staining ($Gars^{C201R/+}$, 114.2 ± 2.5% versus $Gars^{Nmf249/+}$, 124.9 ± 4.6%) ($P < 0.05$, Sidak's multiple comparisons test). This finding indicates that the DRG phenotype correlates with the severity of the *Gars* allele. Moreover, no differences in activated caspase 3 were observed between wild-type and $Gars^{Nmf249/+}$ ganglia (*SI Appendix*, Fig. S5*D*), once again suggesting that cell death is unlikely to be a major contributor to this cellular phenotype.

Mutant Mechanoreceptors and Proprioceptors Are Equally Affected, as Are Nociceptor Subtypes. NF200 and peripherin staining can narrow down sensory neuron classification, but cannot pinpoint function. We therefore used additional markers that broadly relate to the relayed sensory cues. Medium-to-large area neurons positive for NF200 can be subdivided into two main classes based on the absence or presence of parvalbumin (*SI Appendix*, Fig. S2*A*). Sensory neurons expressing NF200, but lacking parvalbumin are largely regarded as mechanosensitive cells, whereas those $NF200^{+}$ neurons coexpressing parvalbumin are proprioceptive (26, 27). Parvalbumin also labels a small population of low threshold cutaneous mechanoreceptive neurons, so there is the minor caveat that not all $parvalbumin^{+}$ neurons are proprioceptive (43). Small area, peripherin-expressing neurons can also be divided into nonpeptidergic, principally mechanical nociceptors and peptidergic, mainly thermal nociceptors based on the binding of isolectin B_4 (IB4) and the expression of calcitonin gene-related peptide (CGRP), respectively (*SI Appendix*, Fig. S2*A*) (44–46). However, ablation of $CGRP^{+}$ neurons has an effect on a small proportion of the $IB4^{+}$ population (47). Wild-type and $Gars^{C201R/+}$ DRG sections were first stained with βIII-tubulin (blue), NF200 (red), and parvalbumin (green), and the percentage of $NF200^{+}$ cells expressing parvalbumin was assessed (Fig. 2*H* and *SI Appendix*, Fig. S2*C*). There was no difference between genotypes in the expression of parvalbumin (Fig. 2*I*), suggesting that, because there are fewer $NF200^{+}$ cells in mutant DRG, mechanoreceptive and proprioceptive neurons are equally affected by mutant *Gars*. Wild-type and $Gars^{C201R/+}$ DRG also showed similar percentages of $peripherin^{+}$ (blue) cells either binding IB4 (green) or expressing CGRP (red) (Fig. 2 *J* and *K* and *SI Appendix*, Fig. S2*D*), suggesting that different subtypes of nociceptor are also equally affected in mutant mice.

Peripheral but Not Central Sensory Nerve Endings Are Anatomically Altered in $Gars^{C201R/+}$ Mice. DRG neurons possess a single axon that projects from the cell body before bifurcating and sending one branch distally to peripheral tissues and another centrally to the dorsal horn of the spinal cord. Given the altered frequencies of large and small area DRG neurons found in CMT2D mice (Figs. 1 and 2 and *SI Appendix*, Figs. S3 and S5), both distal and central sensory nerve endings were analyzed. As mutant ganglia possess fewer $NF200^{+}$ cells, we hypothesized that proprioceptive nerve endings would be impaired. We therefore performed serial transverse sectioning along the entire length of 1-mo-old wild-type and $Gars^{C201R/+}$ soleus muscles to assess muscle spindle number and architecture. Spindles are highly specialized terminals of proprioceptive neurons sensing muscle contraction. Sections were stained with DAPI (blue), SV2/2H3 (green), and laminin (red), to identify nuclei, spindles, and the basement membrane, respectively (Fig. 3*A*). The SV2/2H3 antibody combination identified spindles, as assessed by their stereotypical architecture, whereas additional antibodies against the classic spindle markers parvalbumin and Vglut1 were ineffective (*SI Appendix*, Table S2). Consistent with the reduced number of $NF200^{+}/parvalbumin^{+}$ DRG sensory neurons (Fig. 2), mutant mice had significantly fewer spindles per soleus muscle (Fig. 3*B*), whereas wild-type counts were similar to previously reported (48). Furthermore, we found a dramatic decrease in the percentage of fully innervated spindles (Fig. 3*C*).

As there are also significantly more peripherin-expressing, pain-sensing neurons in mutant DRG (Fig. 2), we also assessed nociceptor termini in the skin. Plantar punches of the hind paws were sectioned and stained from 1-mo-old mice, and the percentage of coverage of the superficial dermis by the axonal marker PGP9.5 was assessed (green, Fig. 3*D*). This method was preferred to intraepidermal nerve fiber counts because it allows a more accurate comparison across different ages. We saw an increase in the peripheral nociceptor innervation in mutant animals (Fig. 3*E*). Although this result did not quite reach significance when tested in isolation (Fig. 3*E*), when analyzed with data from additional time points, it was significant (*SI Appendix*, Fig. S8*B*). The cellular DRG phenotypes of 1-mo-old mutant animals, therefore, correlate with distal proprioceptive and nociceptive sensory neuron deficiencies.

In addition to targeting different peripheral regions for sensing the external environment, sensory neuron subtypes relay their signals to distinct, partially overlapping spinal cord laminae in the dorsal horn. Nociceptors generally form synapses in superficial laminae, numbered I–II, mechanosensitive neurons terminate in deeper laminae III–V, and proprioceptive nerves directly connect centrally and ventrally with interneurons and motor neurons, respectively (27). We therefore sectioned and stained the lumbar spinal cord of 1-mo-old mice for the postsynaptic protein PSD95 (green) and the presynaptic marker synaptophysin (red) to identify and count synapses in laminae I–III (*SI Appendix*, Fig. S6 *A* and *B*). Sensory synapses within dorsal laminae IV–V, central, and ventral regions are more widely dispersed and intermingle with a greater number of nonsensory synapses, thus making them more difficult to accurately quantify, so there is the caveat that these analyses do not cover all sensory subtypes. Furthermore, these synapses are not necessarily all sensory. IB4 (blue) was also applied to the sections to aid in the anatomical identification of the different laminae. Using PSD95, we saw no difference between wild-type and mutant synaptic density per 100 μm^2 of lamina I, outer lamina II

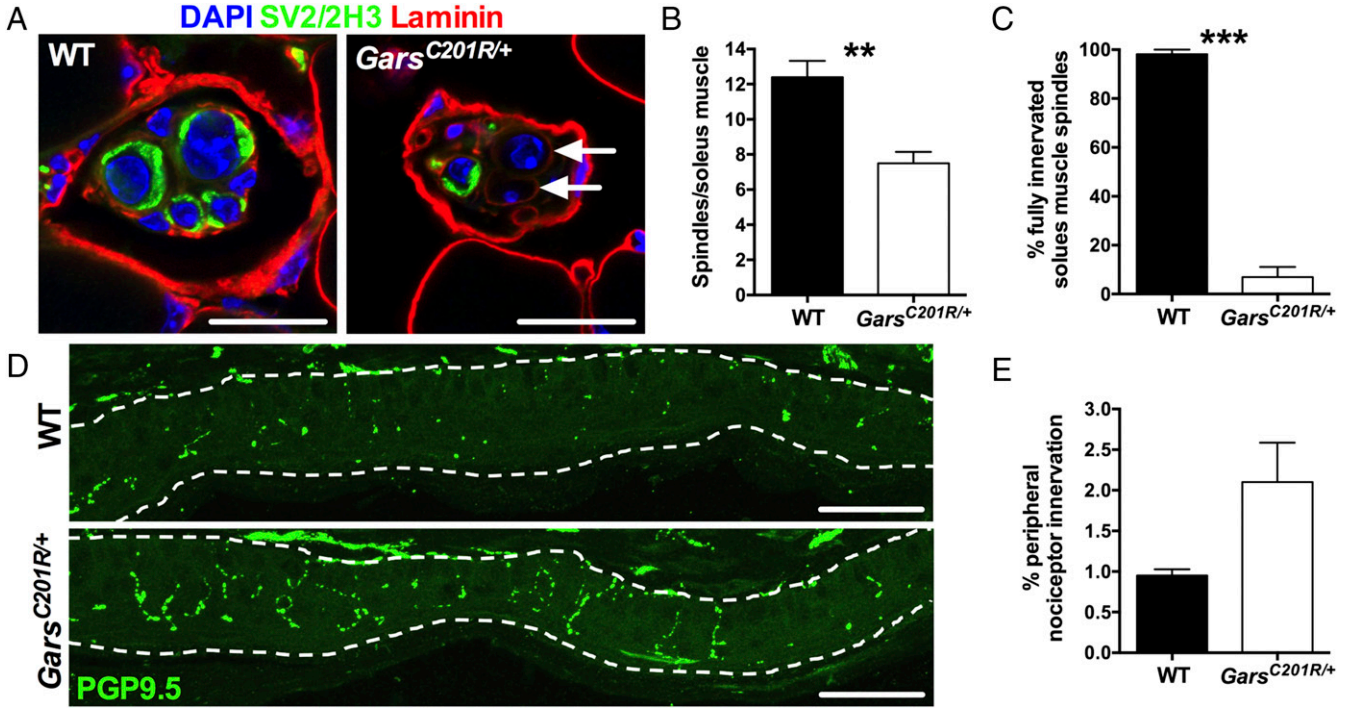

Fig. 3. Peripheral nerve endings are altered in $Gars^{C201R/+}$ mice. (*A*) Representative SV2/2H3$^+$ (green) muscle spindles from wild-type (*Left*) and $Gars^{C201R/+}$ soleus muscles. Antilaminin highlights the muscle basement membrane (red). Note the lack of SV2/3H3 positivity surrounding the central nuclei (DAPI, blue) of the mutant spindle (arrows). Images are single confocal sections. (*B* and *C*) $Gars^{C201R/+}$ mice have significantly fewer spindles per soleus muscle (*B*, $^{**}P = 0.005$, unpaired *t* test). Furthermore, mutant spindles display significant denervation (*C*, $^{***}P < 0.001$, unpaired *t* test). (*D*) Representative collapsed z-stack images taken of the central region of the ventral edge of glabrous hind paw of wild-type (*Top*) and $Gars^{C201R/+}$ mice. Intraepidermal nerve fibers are stained with axonal marker PGP9.5 (green), the epidermis is delineated by dashed lines, and the ventral paw surface is facing down. (*E*) Although not significantly different when tested in isolation ($P = 0.057$, unpaired *t* test), mutant mice show a significant ($P < 0.05$) increase when multiple time points are included in the analysis and data are tested with Sidak's multiple comparisons test (*SI Appendix*, Fig. S8*B*). $n = 4$–5. [Scale bars, 20 μm (*A*) and 50 μm (*D*).] See also *SI Appendix*, Fig. S6.

(IIo), inner lamina II (IIi), or lamina III (*SI Appendix*, Fig. S6*C*, *Left*). This result was replicated using synaptophysin (*SI Appendix*, Fig. S6*C*, *Right*), suggesting that despite *Gars* mice having distorted proportions of sensory subtypes in DRG, homeostatic mechanisms regulate afferent entry into the spinal cord to maintain consistent synapse numbers.

Afferent Neuron Imbalance Determines Deficits in Mutant Sensory Behavior. Subtle alterations in the relative abundance of sensory subtypes may or may not cause macroscopic phenotypes and therefore be biologically relevant; we consequently performed four different sensory behavioral tests that broadly depend upon the sensory neuron subtypes that we have assessed in DRG (*SI Appendix*, Fig. S2*A*). The von Frey test employs monofilaments of increasing rigidity that are used to apply a specific mechanical stimulus to the hind paws of mice. A response to this test is mediated, at least in part, by NF200$^+$/parvalbumin$^-$ neurons. The beam-walking test involves filming mice as they run along a long, thin beam and then using the videos to assess the percentage of correct foot placements. Among other things, this test evaluates the proprioception abilities, and thus the functioning of NF200$^+$/parvalbumin$^+$ neurons. The Randall–Selitto test assesses a withdrawal response to noxious mechanical stimuli of increasing force either on the hind paw or tail, which requires the activation of mechanical nociceptors, which have been suggested to be non-peptidergic fibers (i.e., peripherin$^+$/IB4$^+$/CGRP$^-$ neurons) (46). Finally, the Hargreaves test examines the function of thermal nociceptors postulated to be the peptidergic fibers (peripherin$^+$/IB4$^-$/CGRP$^+$ neurons) (46), using a noxious heat source on the hind paws and measuring the latency to withdrawal. These four tests were performed on 1- and 3-mo-old wild-type and $Gars^{C201R/+}$ mice cohorts (Fig. 4 and *SI Appendix*, Table S3–S7). The 3-mo time point was chosen as a later symptomatic age and to provide a useful comparison with previously generated neuromuscular data (28). Concordant with the significantly reduced numbers of NF200-expressing DRG neurons, mutant animals displayed significant defects in reflex withdrawal to a von Frey stimulus at 3 mo and dysfunctional proprioception at both time points (Fig. 4 *A* and *B*). Moreover, *Gars* mice showed significant hypersensitivity to both noxious mechanical and thermal stimuli at 1 and 3 mo (Fig. 4 *C* and *D*), consistent with the increased numbers of peripherin$^+$ cells in the DRG. When comparing 1- and 3-mo relative values for $Gars^{C201R/+}$, only the beam-walking test became progressively worse.

We also performed motor behavior testing at the same time points, to see whether motor deficits may be contributing to the observed sensory behavior phenotypes (*SI Appendix*, Fig. S7 and Tables S8 and S9). Grip strength tests were performed to simultaneously assess fore and hind limb muscle force and the accelerating rotarod was implemented to measure the complex relationship between motor ability, balance, coordination, and proprioception. We found that both female and male mutant mice showed significant defects in both tests, but, like the sensory phenotypes, these defects did not appear to worsen with age. These results suggest that motor deficiencies may indeed contribute to the mechanosensation and proprioception deficits seen in the $Gars^{C201R/+}$ mice (Fig. 4 *A* and *B*). However, given that the beam-walking deficit, but not the grip strength defect, is progressive from 1 to 3 mo, it appears as though the defective proprioception is partially independent of motor impairment. Furthermore, given that mutant animals respond quicker to noxious stimuli (Fig. 4 *C* and *D*), the motor defects are unlikely to be integral to the pain hypersensitivity.

In summary, the behavioral testing shows that *Gars* mice display multiple disturbances of sensory behavior that correlate with the cellular phenotypes observed in DRG. It is worth emphasizing that the mutants showed a previously unreported phenotype

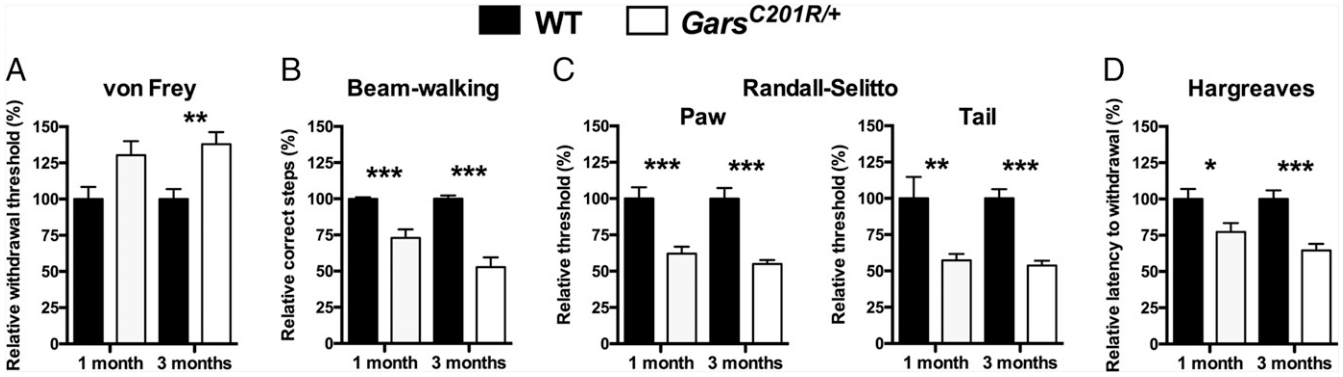

Fig. 4. *Gars*$^{C201R/+}$ mice display multiple sensory behavior defects consistent with the distorted DRG cellular phenotype. (*A*) The force required to elicit a response in the von Frey test is significantly greater for *Gars*$^{C201R/+}$ mice, suggestive of a deficit in mechanosensation. Two-way ANOVA ($P < 0.001$, age; $P < 0.001$, genotype; $P = 0.369$, interaction). This defect does not worsen over time ($P = 0.559$, unpaired *t* test). (*B*) In the beam-walking test, mutant mice make significantly more incorrect hind paw steps, perhaps due to defective proprioception. $P < 0.001$, Kruskal–Wallis test, ***$P < 0.001$ Dunn's multiple comparison test. This deficiency is exacerbated from 1 to 3 mo ($P = 0.030$, unpaired *t* test). (*C*) In stark contrast to the von Frey test results, mutant mice display hypersensitivity to noxious mechanical stimuli on both the hind paw ($P = 0.514$, age; $P < 0.001$, genotype; $P = 0.347$, interaction, two-way ANOVA) and tail ($P < 0.001$, age; $P < 0.001$, genotype; $P = 0.138$, interaction, two-way ANOVA), as assessed by the Randall–Selitto test. These defects do not worsen with time ($P = 0.177$ and 0.505, unpaired *t* test). (*D*) Mutant mice also respond faster than wild-type animals to a painful heat source directed to the hind paw, indicative of hypersensitivity to noxious thermal stimuli. Two-way ANOVA ($P = 0.017$, age; $P < 0.001$, genotype; $P = 0.109$, interaction). The defect does not worsen over time ($P = 0.103$, unpaired *t* test). *$P < 0.05$, **$P < 0.01$, ***$P < 0.001$, Sidak's multiple comparisons test (*A*, *C*, and *D*). $n = 15$–18 (*A*, *B*, and *D*), and $n = 11$–13 (*C*). The statistical tests represented on the figures were performed on raw data (*SI Appendix*, Tables S3–S7), whereas the percentages relative to wild type, which are plotted, were used to compare mutant progression over time. See also *SI Appendix*, Fig. S7 and Tables S8 and S9.

of reduced mechanosensation (Fig. 4*A*) with the contrasting enhancement of mechanical nociception (Fig. 4*C*).

***Gars*$^{C201R/+}$ Mice Display Developmental Sensory Deficits.** To see whether the cellular sensory phenotype gets progressively worse with time, we analyzed DRG from 1 d (postnatal day 1, P1) and 3-mo-old mice. We were again able to demonstrate at both time points the presence of significantly fewer mutant NF200$^+$ neurons (Fig. 5*A*) and more peripherin$^+$ cells (Fig. 5*B*), confirming the 1-mo result. Comparing the percentages of NF200$^+$ and peripherin$^+$ cells in mutant samples relative to wild type, we see no significant differences at any of the time points ($P > 0.05$, Sidak's multiple comparisons test). We have thus shown that the disturbed population of sensory neuron subtypes resident in the mutant DRG are present at birth and do not change by early adulthood. Cleaved-caspase 3 levels also did not differ, suggesting that cell death is playing no major role in the onset and/or maintenance of this phenotype (*SI Appendix*, Fig. S8*A*).

We also assessed intraepidermal nerve fiber density at P1 and 3 mo. Contrasting with the 1-mo data, we saw no difference between wild type and mutant at these early and late time points (*SI Appendix*, Fig. S8*B*). Innervation density declines over time in both mutant and wild-type animals; however, it appears to take longer in the *Gars*$^{C201R/+}$ mice.

To confirm whether sensory nerve development is affected in *Gars* mutant mice, we analyzed axonal projections of small-diameter sensory neurons in wholemount hind paws of E13.5 embryos (49, 50). To assess axonal extension, we measured the distance from the main nerve trunk termini innervating the foot plate to the tips of the embryonic digits (Fig. 5*C*). We saw no difference in either the ventral (Fig. 5*D*) or the dorsal (Fig. 5*E*) nerve, indicating that nerve terminal extension is unaffected. However, we found that mutant nerves display a significant reduction in branch density in the dorsal floor plate (Fig. 5*F*). This finding suggests that arborization of mutant nociceptive neurons is impaired (51), and that *Gars*$^{C201R/+}$ mice display developmental perturbations in the sensory nervous system.

Mutant Thermal Nociceptors Display Greater Excitability. Cell autonomous differences in neuronal excitability (12) may contribute to the pain hypersensitivity phenotype of *Gars* mice. We therefore cultured DRG neurons from 1-mo-old animals and performed calcium imaging experiments using the ratiometric calcium indicator fura-2 (52). We saw no difference in the baseline fura-2 ratio between wild-type and *Gars*$^{C201R/+}$ sensory neurons (0.840 ± 0.012 versus 0.835 ± 0.014, $P = 0.787$, unpaired *t* test), suggestive of equivalent resting state calcium levels in wild-type and mutant neurons. When 50 mM KCl was applied to the cells to trigger depolarization, there was also no difference in the elicited response (Fig. 6 *A* and *B*). In these live DRG cultures, NF200$^+$ and peripherin$^+$ neurons cannot be readily differentiated. We therefore applied 1 μM capsaicin, which activates the nonselective cation channel TRPV1 (53), to functionally differentiate thermal nociceptors. Addition of capsaicin induced a greater relative change in the fura-2 ratio of capsaicin-responsive *Gars*$^{C201R/+}$ than wild-type neurons (Fig. 6 *A* and *C*), perhaps indicative of TRPV1 up-regulation in mutant thermal nociceptors. We thus stained 1-mo-old wild-type and mutant *Gars* DRG sections with anti-TRPV1 and measured the mean fluorescence intensity in TRPV1$^+$ neurons selected by uniform thresholding across samples (Fig. 6 *D* and *E*). *Gars*$^{C201R/+}$ DRG showed a significant increase in TRPV1 expression compared with wild type, whereas the more severe mutant, *Gars*$^{Nmf249/+}$, showed an even greater mean intensity (Fig. 6*D*). These experiments therefore indicate that mutant thermal nociceptors are intrinsically hyperresponsive to painful stimuli due to an increase in TRPV1 expression, which is likely to contribute to the pain hypersensitivity phenotype observed in adult *Gars*$^{C201R/+}$ mice.

Mutant GlyRS Aberrantly Binds the Trk Receptors and Activates Trk Signaling. CMT2D-linked mutations in *GARS* have previously been shown to confer neomorphic binding activity on mutant GlyRS, causing it to interact with an extracellular domain of Nrp1 and block VEGF signaling (18). As tropomyosin receptor kinase (Trk) receptors play a key role in sensory neuron development and differentiation (54), and sensory neuron fate is perturbed in CMT2D mice, we hypothesized that mutant GlyRS may also spuriously interact with one or more of the Trk receptors. We thus performed in vitro pull-down experiments using the mouse motor neuron-like NSC-34 cell line transfected with V5-tagged wild-type and two mutant forms of GlyRS (P234KY and C157R, human equivalents of the severe, P278KY, and mild, C201R, *Gars* mouse mutations, respectively). Using Fc-tagged recombinant TrkA, TrkB, and TrkC, both P234KY and C157R, but not wild-type GlyRS, were shown to interact with all three Trk receptors (Fig. 7*A*). Moreover, the extent

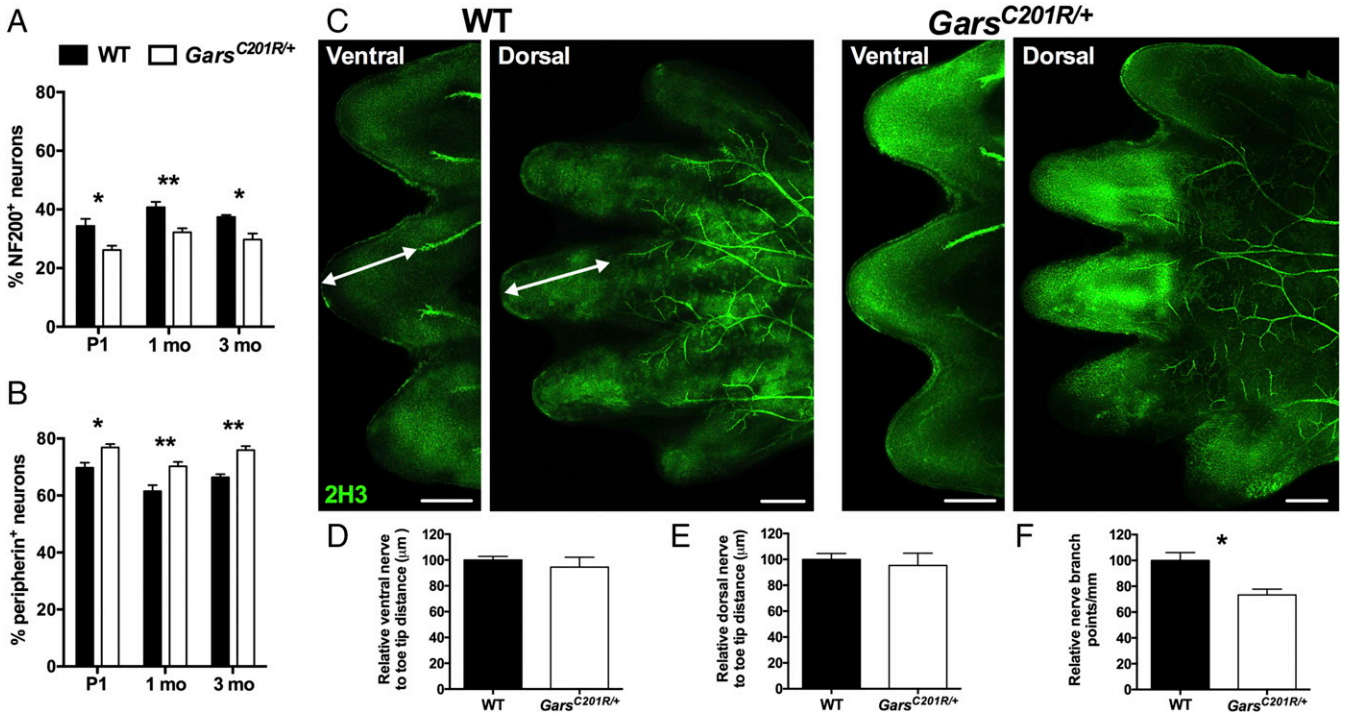

Fig. 5. *Gars*$^{C201R/+}$ sensory neurons display developmental defects. (*A*) *Gars* mutant DRG display significantly smaller percentages of NF200^{+} cells at P1, 1 mo, and 3 mo, suggestive of a nonprogressive, prenatal defect. The average percentage of NF200^{+} cells in mutant DRG is 74.4% (P1), 79.1% (1 mo), and 79.4% (3 mo) relative to wild type. Two-way ANOVA ($P = 0.011$, age; $P < 0.001$, genotype; $P = 0.973$, interaction). (*B*) Mutant DRG show a reciprocal increase in the percentage of cells expressing peripherin at all three time points. The mean percentage of peripherin^{+} cells in mutant DRG relative to wild type is 110.9% (P1), 114.2% (1 mo), and 114.3% (3 mo). Two-way ANOVA ($P < 0.001$, age; $P < 0.001$, genotype; $P = 0.769$, interaction). Statistical analyses are performed on raw data and not percentages relative to wild type (*A* and *B*). $*P < 0.05$, $**P < 0.01$, Sidak's multiple comparisons test (*A* and *B*). (*C*) Representative single confocal plane, tile scan images of ventral and dorsal aspects of wild-type and *Gars*$^{C201R/+}$ E13.5 hind paws stained for neurofilament (2H3, green). The arrows depict distances from the major nerve branches to the tips of the toes measured in *D* and *E*. (Scale bars, 250 μm.) (*D*–*F*) There was no difference between wild-type and mutant mice in the targeting of sensory nerves to the hind paw extremities on ventral (*D*, $P = 0.413$, unpaired *t* test) or dorsal (*E*, $P = 0.629$, unpaired *t* test) sides. However, *Gars*$^{C201R/+}$ neurons display reduced branching in the dorsal foot plate (*F*, $*P = 0.0376$, unpaired *t* test). Statistical analyses were performed on percentage values relative to the wild-type mean. $n = 3$–9. See also *SI Appendix*, Fig. S8.

of binding appeared to correlate with mutant severity for TrkB and TrkC. To determine the impact of this anomalous binding, N2a neuroblastoma cells stably overexpressing FLAG-tagged TrkB (Fig. 7*B*) (55) were exposed to recombinant wild-type, L129P, and G240R GlyRS proteins in the media. The *GARS*^{L129P} and *GARS*^{G240R} mutations were chosen because they are two of the most tightly linked to human neuropathy (9). Both mutant GlyRS proteins caused an increase in ERK1/2 phosphorylation (Fig. 7*C*), which is an integral part of the Trk signaling cascade (56). Interestingly, extracellular wild-type GlyRS has previously been shown to decrease ERK phosphorylation in a time- and dose-dependent fashion in the human carcinoma cell line, HCT116, functioning as a tumor-defense system (19); however, consistent with our result (Fig. 7*C*), this effect was not observed in the human neuroblastoma cell line, SH-SY5Y (19).

Discussion

Patients with CMT2D display both motor and sensory pathology, yet the sensory component has received little attention both in humans and animal models. We therefore performed a detailed examination of the sensory nervous system of CMT2D mice to better understand the afferent nerve pathogenesis (see *SI Appendix*, Fig. S9 for a phenotypic overview). We found that mutant DRG possess fewer large diameter, NF200^{+} cells and a concomitant increase in the number of small diameter, peripherin^{+} neurons (Figs. 1 and 2), a phenotype that nicely correlates with CMT2D mutant severity (*SI Appendix*, Fig. S5) and alterations in sensory behavior (Fig. 4). Assessment of activated caspase 3 levels and DRG neuron counts indicate that this phenotype is unlikely to be caused by postnatal cell death or defective neural crest migration and survival, but is rather a developmental sensory subtype switch (*SI Appendix*, Fig. S3). Consistent with a prenatal onset, the DRG phenotype is present at birth (Fig. 5 *A* and *B*). Although we do not directly show that sensory identity is perturbed during embryonic development, we do observe defective sensory nerve branching in the mutant hind paw at E13.5 (Fig. 5*F*), similar to the previously reported embryonic impairment in facial motor neuron migration (18) and suggestive of developmental onset. However, the subtype identity defect appears to be sensory specific, as mutant *Gars* mice do not show a difference in the proportion of α- and γ-motor neurons (*SI Appendix*, Fig. S4). Using several markers for sensory function, we observed that mechanoreceptive and proprioceptive neurons are equally affected by *Gars* mutation, as are nonpeptidergic and peptidergic nociceptors (Fig. 2). The pathological effect of mutant GlyRS could therefore be triggered by the differential expression of specific genes vital to sensory diversification between the mutually exclusive NF200^{+} and peripherin^{+} neuronal populations (e.g., Trk receptors) (57). Differences in cellular origin or timing of gene expression leading to subtype specification could also contribute to the DRG phenotype and explain the lack of motor subtype distortion (58, 59).

CMT2D-associated mutant GlyRS was recently shown to aberrantly bind to the neuronal receptor protein NRP1 and antagonize its activity (18). Although NRP1 was the focus of that study, mutant GlyRS was shown to interact with a number of other proteins found on the neuronal surface, albeit to a lesser degree (18). One of these proteins was TrkB, a neurotrophin receptor that, once activated, specifically drives differentiation and survival of mechanosensitive sensory neurons (60). Similarly, TrkA and TrkC are pivotal to the survival of nociceptive and proprioceptive nerves, respectively (61, 62). We therefore performed in vitro pull-down experiments and

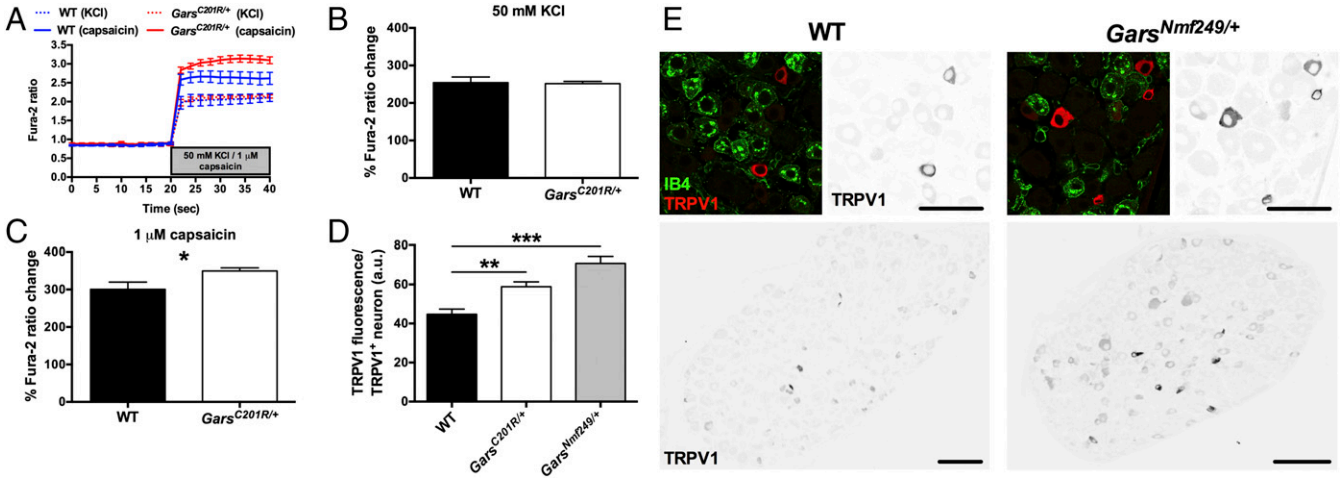

Fig. 6. Thermal nociceptors from mutant *Gars* mice are hyperexcitable. (*A*–*C*) One-month old wild-type (*A*, blue, dashed line) and mutant (*A*, red, dashed line) primary DRG neurons show no difference in their responses to 50 mM KCl 24 h postplating (*B*, $P = 0.864$, unpaired *t* test), as assessed using the ratiometric calcium indicator fura-2. However, the increase in cytosolic calcium upon stimulation by 1 μM capsaicin is greater in $Gars^{C201R/+}$ than wild-type neurons (*A*, solid lines). Wild-type and mutant cells display similar baseline calcium levels (*A*), but capsaicin triggers a significantly larger increase in the fura-2 ratio ($I_{340\ nm}/I_{380\ nm}$) in $Gars^{C201R/+}$ neurons (*C*, $*P = 0.0236$, unpaired *t* test). Only data generated from capsaicin-responsive cells (i.e., thermal nociceptors) are included in these graphs (*A* and *C*). (*D*) The capsaicin receptor, TRPV1, is up-regulated in $Gars^{C201R/+}$ and $Gars^{Nmf249/+}$ DRG compared with wild type and correlates with mutant severity ($P < 0.001$, one-way ANOVA). $**P < 0.01$, $***P < 0.001$, Sidak's multiple comparisons test. (*E*) Representative single plane, tile scan confocal images of 1-mo-old wild-type (*Left*) and $Gars^{Nmf249/+}$ DRG stained with anti-TRPV1 (red) and IB4 (green). $n = 4$–8. [Scale bars, 50 μm (*Top*) and 100 μm (*Bottom*).]

showed that two mutants, but not wild-type GlyRS, aberrantly bind to TrkA, TrkB, and TrkC (Fig. 7*A*). This binding likely accounts for the misactivation of TrkB signaling in N2a neuroblastoma cells caused by application of mutant GlyRS to the media (Fig. 7*C*). A previous study has shown that expression of TrkC from the *TrkA* locus caused a developmental fate switch in DRG sensory subtypes (63). Given that GlyRS is expressed during early development (11, 12), and that arborization of nociceptive neurons is developmentally impaired in CMT2D mice (Fig. 5*F*), our work has identified a highly plausible mechanism to account for the sensory neuron identity defects observed in *Gars* animals; namely, mutant GlyRS binds and spuriously activates multiple Trk receptors, thereby subtly subverting sensory neuron differentiation and/or survival during early stages of development. These in vitro experiments add three additional neuronal receptors (TrkA–C) to the list of now four proteins (including NRP1) to which mutant GlyRS convincingly binds, providing further rationale for the neuronal specificity of this disease, despite *GARS* being a widely expressed housekeeping gene. Furthermore, *GARS* provides a fascinating example of how gain-of-function mutations can cause a protein to aberrantly interact with multiple different pathways, resulting in either their activation or down-regulation. This list might be far from complete, and future experiments will investigate what additional proteins mutant GlyRS is capable of interacting with.

Regardless of the cause of the afferent imbalance in mutant DRG, it is clear that it represents a major, nonprogressive, developmental component of the sensory phenotype of CMT2D mice. This is in agreement with the sensory alterations of *Gars* mice not worsening from 1 to 3 mo (except for proprioception, Fig. 4), and congruent with $Gars^{C201R/+}$ sensory saphenous nerve showing a smaller average axon caliber, but no signs of degeneration or axon loss for up to 3 mo (12). Consistent with this finding, the extent of CMT2D patient sensory deficiency is reported to be reliant upon disease severity and not duration (20). There are only limited clinical data on the sensory symptoms of patients with CMT2D, perhaps due to the motor phenotype being more severe. It is therefore possible that the nonprogressive perturbation in sensory fate is also seen in patients with CMT2D resulting in subtle, undiagnosed sensory symptoms before the manifestation of motor deficits and limited sensory degeneration during adolescence. Accordingly, without the initial developmental perturbation of the sensory system, afferent pathology may simply not occur, which could explain the predominantly motor presentation of patients with dSMA-V. An element of mutant *GARS*-related sensory pathology may therefore be binary (present/absent) and independent from the neurodegeneration; if mutant GlyRS triggers the initial developmental insult, CMT2D will arise, but if not, then dSMA-V manifests.

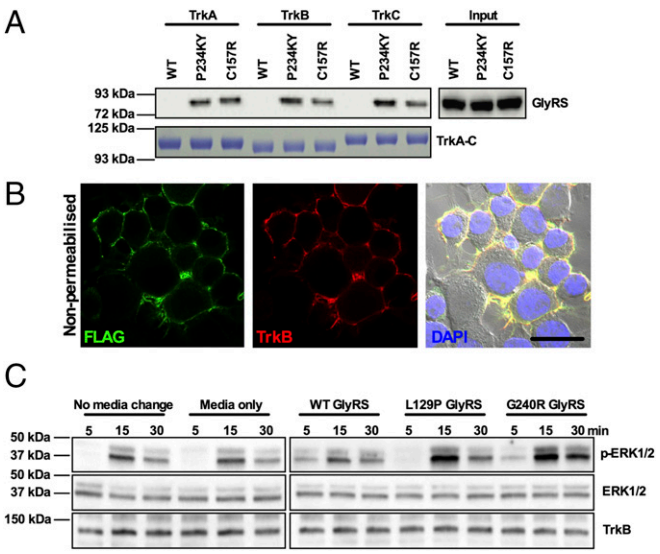

Fig. 7. Mutant GlyRS binds to Trk receptors and activates Trk signaling. (*A*) In vitro pull-down assay showing aberrant P234KY and C157R, but not wild-type, GlyRS interaction with TrkA, TrkB, and TrkC. (*B*) Representative single plane confocal and phase contrast (with DAPI) image of nonpermeabilized N2a cells stably overexpressing FLAG-TrkB (green). (Scale bar, 20 μm.) (*C*) Representative Western blot of lysates from N2a cells exposed for 5, 15, and 30 min to 150 nM recombinant wild-type and mutant (L129P and G240R) GlyRS added to the extracellular medium. Cells treated with either GlyRS mutant showed increased ERK1/2 phosphorylation compared with the media-only control, whereas wild-type GlyRS had no such effect. Note that the total levels of ERK1/2 and TrkB vary very little among samples.

In addition to a prenatal developmental disturbance, maturation and degenerative pathways are also contributing to GlyRS-mediated pathology. *Gars*$^{C201R/+}$ mice possess significantly fewer muscle spindles and reduced innervation per spindle (Fig. 3 *B* and *C*), which is probably reflective of reduced formation during development and subsequent degeneration. Together with the previously reported decrease in amplitude of sensory nerve action potentials (SNAPs) in large area neurons (1.7 ± 0.2 μV versus 1.2 ± 0.2 μV) (12), both defects are likely to contribute to the defective proprioception, whereas progressive distal nerve deterioration perhaps accounts for proprioception being the only sensory behavior to decline over time (Fig. 4*B*). Therefore, it is conceivably not a coincidence that the ability of patients with CMT2D to sense vibration is the most impaired sensory symptom.

We have previously shown that a developmental delay in NMJ maturation precedes synaptic degeneration in *Gars* mouse distal muscles (28). Interestingly, we see a similar pruning deficiency in the intraepidermal nociceptors of the mutant hind paws (*SI Appendix*, Fig. S8*B*). We believe that this observation represents impairment of the early postnatal refinement of sensory architecture (64) (akin to the motor phenotype) as opposed to degeneration, as the latter would likely precipitate a reduction in the pain hypersensitivity phenotype by 3 mo. To find an alternate explanation, we performed synapse counts in distinct spinal cord dorsal laminae (*SI Appendix*, Fig. S6) and calcium imaging experiments on primary DRG cultures (Fig. 6). We saw no difference between genotypes in dorsal horn synapse densities (*SI Appendix*, Fig. S6*C*). This finding suggests that homeostatic mechanisms are at work to restrict C-fiber entry into the spinal cord and that there is perhaps an excess of NF200^{+} neuronal branches targeting dorsal laminae in wild-type mice. Nevertheless, dorsal horn synapse counts do not assess synaptic strength and therefore it is uncertain whether or not central sensitization has occurred. To assess this question peripherally, we analyzed cytosolic calcium dynamics and found that mutant thermal nociceptors are more responsive to capsaicin than wild-type neurons (Fig. 6 *A* and *C*), and that this is likely due to increased expression of the capsaicin receptor protein TRPV1 (Fig. 6 *D* and *E*). The increased number of small area neurons and axons probably account for the previously reported (nonsignificant) increase in mutant C-fiber SNAP amplitude (312 ± 60 μV versus 474 ± 123 μV) (12). Through activity-dependent mechanisms of peripheral or central plasticity, such as differential ion channel expression/phosphorylation (Fig. 6 *D* and *E*) or synaptic potentiation (65), we hypothesize that the abundance of small area neurons could alter neuronal excitability and at least partly explain the inherent thermal nociceptor hyperexcitability and the pain hypersensitivity phenotypes.

In summary, we have shown that CMT2D mice display numerous sensory symptoms that hinge upon a disturbed equilibrium between functional subtypes of afferent neurons, which is likely caused by aberrant binding of mutant GlyRS to Trk receptors resulting in altered Trk signaling. This phenotype is likely developmental in origin and could serve to explain the variable sensory pathology of *GARS*-associated neuropathy. In light of the range of deficits reported in *Gars* mice, we propose that CMT2D pathology reflects a complex interplay between developmental, maturation, and survival pathways, a conclusion that has profound implications for the development of novel therapies and timing of therapeutic intervention for the treatment of this disease.

Materials and Methods

Animals and Cell Culture. *Gars*$^{C201R/+}$ handling and experiments were performed under license from the United Kingdom Home Office in accordance with the Animals (Scientific Procedures) Act (1986), and approved by the University College London, Institute of Neurology ethics committee for work in London, and by the University of Oxford ethical review panel for experiments conducted in Oxford. *Gars*$^{Nmf249/+}$ mouse husbandry and procedures were conducted in accordance with the NIH Guide for Care and Use of Laboratory Animals and approved by The Jackson Laboratory animal care and use committee. To reduce the overall number of mice used, multiple tissues were harvested from both males and females used for behavioral testing and other parallel studies (66). Immortalized cell lines were grown in Dulbecco's modified Eagle medium (DMEM) (Thermo Fisher Scientific, 41966) as previously described (67). DRG were dissected (68), cultured (69), and immunofluorescence was performed (67) as published, with minor modifications. Further details of animal and cell culture maintenance and experiments are outlined in *SI Appendix, SI Materials and Methods*.

Immunohistochemistry. For immunofluorescence analysis, all tissues were fixed in 4% (wt/vol) paraformaldehyde (PFA, Electron Microscopy Sciences) in PBS, before equilibrating in 20% (wt/vol) sucrose (Sigma, S7903), embedding in Tissue-Tek OCT compound (Sakura Finetek, 4583), and sectioning with an OTF Cryostat (Bright Instruments). Subtle variations in this protocol for each tissue type are reported in *SI Appendix, SI Materials and Methods*. For staining, sections were encircled with a hydrophobic barrier pen (Dako, S2002) on microscope slides, and processed in a similar manner as the DRG cultures (see *SI Appendix, SI Materials and Methods* for procedure details). E13.5 hind feet were removed from embryos between the ankle and knee joints and processed, with subtle modifications outlined in *SI Appendix, SI Materials and Methods* as previously described (49). Protein lysates were generated from DRG and immortalized cell lines, and pull-down experiments and Western blot analysis were performed using published protocols (18, 67) with minor modifications summarized in *SI Appendix, SI Materials and Methods*. Primary (*SI Appendix*, Tables S1 and S2) and secondary antibodies used in this study are outlined in *SI Appendix, SI Materials and Methods*. Cells and tissues were imaged and analyzed using standard protocols that are described in detail in *SI Appendix, SI Materials and Methods*.

Sensory and Motor Behavior Testing. Sensory and motor behavior were assessed as previously described (12, 70–74), with modifications as listed in *SI Appendix, SI Materials and Methods*.

Statistical Analysis. Data were assumed to be normally distributed unless evidence to the contrary could be provided by the D'Agostino and Pearson omnibus normality test. Data were statistically analyzed using an unpaired *t* test, or one- or two-way ANOVA with Sidak's multiple comparisons tests. If the data did not pass normality testing, Mann–Whitney *u* tests or Kruskal–Wallis tests with Dunn's multiple comparison tests were used. GraphPad Prism 6 software was used for all statistical analyses and production of figures. Means + SEM are plotted for all graphs.

ACKNOWLEDGMENTS. We thank members of the G.S., M.Z.C., K.T., D.L.B., and L. Greensmith [Institute of Neurology, University College London (UCL)] laboratories for productive discussions; Andrey Y. Abramov, J. Barney Bryson, Benjamin E. Clarke, Steven Middleton, Gustavo Pregoni, Annina B. Schmid, Greg A. Weir, and Emma R. Wilson for sharing experimental expertise; Nathalie Schmieg for providing the E18.5 *Kidins220*$^{-/-}$ brain; and Alexander M. Rossor for critical reading of the manuscript. This work was supported by Wellcome Trust Sir Henry Wellcome Postdoctoral Fellowship 103191/A/13/Z (to J.N.S.), the French Muscular Dystrophy Association (AFM-Telethon) (J.N.S., M.Z.C., and K.T.), Wellcome Trust Senior Investigator Award 107116/Z/15/Z (to G.S.), UCL (G.S.), a UK Medical Research Council research grant (to J.M.D.), and NIH Grants F31 NS100328, R01NS054154, and R01GM088278 (to E.L.S., R.W.B., and X.-L.Y., respectively).

1. Reilly MM, Murphy SM, Laurá M (2011) Charcot-Marie-Tooth disease. *J Peripher Nerv Syst* 16:1–14.
2. El-Abassi R, England JD, Carter GT (2014) Charcot-Marie-Tooth disease: An overview of genotypes, phenotypes, and clinical management strategies. *PM R* 6:342–355.
3. Skre H (1974) Genetic and clinical aspects of Charcot-Marie-Tooth's disease. *Clin Genet* 6:98–118.
4. Antonellis A, et al. (2003) Glycyl tRNA synthetase mutations in Charcot-Marie-Tooth disease type 2D and distal spinal muscular atrophy type V. *Am J Hum Genet* 72:1293–1299.
5. Jordanova A, et al. (2006) Disrupted function and axonal distribution of mutant tyrosyl-tRNA synthetase in dominant intermediate Charcot-Marie-Tooth neuropathy. *Nat Genet* 38:197–202.
6. Latour P, et al. (2010) A major determinant for binding and aminoacylation of tRNA(Ala) in cytoplasmic Alanyl-tRNA synthetase is mutated in dominant axonal Charcot-Marie-Tooth disease. *Am J Hum Genet* 86:77–82.
7. McLaughlin HM, et al.; NISC Comparative Sequencing Program (2010) Compound heterozygosity for loss-of-function lysyl-tRNA synthetase mutations in a patient with peripheral neuropathy. *Am J Hum Genet* 87:560–566.
8. Vester A, et al.; NISC Comparative Sequencing Program (2013) A loss-of-function variant in the human histidyl-tRNA synthetase (*HARS*) gene is neurotoxic *in vivo*. *Hum Mutat* 34:191–199.
9. Motley WW, Talbot K, Fischbeck KH (2010) *GARS* axonopathy: Not every neuron's cup of tRNA. *Trends Neurosci* 33:59–66.

10. Storkebaum E (2016) Peripheral neuropathy via mutant tRNA synthetases: Inhibition of protein translation provides a possible explanation. *BioEssays* 38:818–829.
11. Seburn KL, Nangle LA, Cox GA, Schimmel P, Burgess RW (2006) An active dominant mutation of glycyl-tRNA synthetase causes neuropathy in a Charcot-Marie-Tooth 2D mouse model. *Neuron* 51:715–726.
12. Achilli F, et al. (2009) An ENU-induced mutation in mouse glycyl-tRNA synthetase (*GARS*) causes peripheral sensory and motor phenotypes creating a model of Charcot-Marie-Tooth type 2D peripheral neuropathy. *Dis Model Mech* 2:359–373.
13. Nangle LA, Zhang W, Xie W, Yang XL, Schimmel P (2007) Charcot-Marie-Tooth disease-associated mutant tRNA synthetases linked to altered dimer interface and neurite distribution defect. *Proc Natl Acad Sci USA* 104:11239–11244.
14. Xie W, Nangle LA, Zhang W, Schimmel P, Yang XL (2007) Long-range structural effects of a Charcot-Marie-Tooth disease-causing mutation in human glycyl-tRNA synthetase. *Proc Natl Acad Sci USA* 104:9976–9981.
15. Motley WW, et al. (2011) Charcot-Marie-Tooth-linked mutant GARS is toxic to peripheral neurons independent of wild-type GARS levels. *PLoS Genet* 7:e1002399.
16. He W, et al. (2011) Dispersed disease-causing neomorphic mutations on a single protein promote the same localized conformational opening. *Proc Natl Acad Sci USA* 108: 12307–12312.
17. Grice SJ, et al. (2015) Dominant, toxic gain-of-function mutations in *gars* lead to non-cell autonomous neuropathology. *Hum Mol Genet* 24:4397–4406.
18. He W, et al. (2015) CMT2D neuropathy is linked to the neomorphic binding activity of glycyl-tRNA synthetase. *Nature* 526:710–714.
19. Park MC, et al. (2012) Secreted human glycyl-tRNA synthetase implicated in defense against ERK-activated tumorigenesis. *Proc Natl Acad Sci USA* 109:E640–E647.
20. Sivakumar K, et al. (2005) Phenotypic spectrum of disorders associated with glycyl-tRNA synthetase mutations. *Brain* 128:2304–2314.
21. Del Bo R, et al. (2006) Coexistence of CMT-2D and distal SMA-V phenotypes in an Italian family with a *GARS* gene mutation. *Neurology* 66:752–754.
22. Hamaguchi A, Ishida C, Iwasa K, Abe A, Yamada M (2010) Charcot-Marie-Tooth disease type 2D with a novel glycyl-tRNA synthetase gene (*GARS*) mutation. *J Neurol* 257:1202–1204.
23. Sun A, et al. (2015) A novel mutation of the glycyl-tRNA synthetase (*GARS*) gene associated with Charcot-Marie-Tooth type 2D in a Chinese family. *Neurol Res* 37:782–787.
24. Lee HJ, et al. (2012) Two novel mutations of *GARS* in Korean families with distal hereditary motor neuropathy type V. *J Peripher Nerv Syst* 17:418–421.
25. Van Langenhove T, van der Zee J, Van Broeckhoven C (2012) The molecular basis of the frontotemporal lobar degeneration-amyotrophic lateral sclerosis spectrum. *Ann Med* 44:817–828.
26. Le Pichon CE, Chesler AT (2014) The functional and anatomical dissection of somatosensory subpopulations using mouse genetics. *Front Neuroanat* 8:21.
27. Lallemend F, Ernfors P (2012) Molecular interactions underlying the specification of sensory neurons. *Trends Neurosci* 35:373–381.
28. Sleigh JN, Grice SJ, Burgess RW, Talbot K, Cader MZ (2014) Neuromuscular junction maturation defects precede impaired lower motor neuron connectivity in Charcot-Marie-Tooth type 2D mice. *Hum Mol Genet* 23:2639–2650.
29. Harper AA, Lawson SN (1985) Conduction velocity is related to morphological cell type in rat dorsal root ganglion neurones. *J Physiol* 359:31–46.
30. Chen XJ, et al. (2007) Proprioceptive sensory neuropathy in mice with a mutation in the cytoplasmic Dynein heavy chain 1 gene. *J Neurosci* 27:14515–14524.
31. Sassone J, et al. (2016) ALS mouse model $SOD1^{G93A}$ displays early pathology of sensory small fibers associated to accumulation of a neurotoxic splice variant of peripherin. *Hum Mol Genet* 25:1588–1599.
32. Sommer EW, Kazimierczak J, Droz B (1985) Neuronal subpopulations in the dorsal root ganglion of the mouse as characterized by combination of ultrastructural and cytochemical features. *Brain Res* 346:310–326.
33. Lawson SN, Harper AA, Harper EI, Garson JA, Anderton BH (1984) A monoclonal antibody against neurofilament protein specifically labels a subpopulation of rat sensory neurones. *J Comp Neurol* 228:263–272.
34. Parysek LM, Goldman RD (1988) Distribution of a novel 57 kDa intermediate filament (IF) protein in the nervous system. *J Neurosci* 8:555–563.
35. Ferri GL, et al. (1990) Neuronal intermediate filaments in rat dorsal root ganglia: differential distribution of peripherin and neurofilament protein immunoreactivity and effect of capsaicin. *Brain Res* 515:331–335.
36. Bae JY, Kim JH, Cho YS, Mah W, Bae YC (2015) Quantitative analysis of afferents expressing substance P, calcitonin gene-related peptide, isolectin B4, neurofilament 200, and Peripherin in the sensory root of the rat trigeminal ganglion. *J Comp Neurol* 523:126–138.
37. Zhao J, et al. (2010) Small RNAs control sodium channel expression, nociceptor excitability, and pain thresholds. *J Neurosci* 30:10860–10871.
38. Lekan HA, Chung K, Yoon YW, Chung JM, Coggeshall RE (1997) Loss of dorsal root ganglion cells concomitant with dorsal root axon sprouting following segmental nerve lesions. *Neuroscience* 81:527–534.
39. Tandrup T, Woolf CJ, Coggeshall RE (2000) Delayed loss of small dorsal root ganglion cells after transection of the rat sciatic nerve. *J Comp Neurol* 422:172–180.
40. Stifani N (2014) Motor neurons and the generation of spinal motor neuron diversity. *Front Cell Neurosci* 8:293.
41. Friese A, et al. (2009) Gamma and alpha motor neurons distinguished by expression of transcription factor Err3. *Proc Natl Acad Sci USA* 106:13588–13593.
42. Spaulding EL, et al. (2016) Synaptic deficits at neuromuscular junctions in two mouse models of Charcot-Marie-Tooth type 2d. *J Neurosci* 36:3254–3267.
43. de Nooij JC, Doobar S, Jessell TM (2013) Etv1 inactivation reveals proprioceptor subclasses that reflect the level of NT3 expression in muscle targets. *Neuron* 77:1055–1068.
44. Alvarez FJ, Morris HR, Priestley JV (1991) Sub-populations of smaller diameter trigeminal primary afferent neurons defined by expression of calcitonin gene-related peptide and the cell surface oligosaccharide recognized by monoclonal antibody LA4. *J Neurocytol* 20:716–731.
45. Scherrer G, et al. (2009) Dissociation of the opioid receptor mechanisms that control mechanical and heat pain. *Cell* 137:1148–1159.
46. Cavanaugh DJ, et al. (2009) Distinct subsets of unmyelinated primary sensory fibers mediate behavioral responses to noxious thermal and mechanical stimuli. *Proc Natl Acad Sci USA* 106:9075–9080.
47. McCoy ES, et al. (2013) Peptidergic CGRPα primary sensory neurons encode heat and itch and tonically suppress sensitivity to cold. *Neuron* 78:138–151.
48. Oliveira Fernandes M, Tourtellotte WG (2015) Egr3-dependent muscle spindle stretch receptor intrafusal muscle fiber differentiation and fusimotor innervation homeostasis. *J Neurosci* 35:5566–5578.
49. Wickramasinghe SR, et al. (2008) Serum response factor mediates NGF-dependent target innervation by embryonic DRG sensory neurons. *Neuron* 58:532–545.
50. Patel TD, Jackman A, Rice FL, Kucera J, Snider WD (2000) Development of sensory neurons in the absence of NGF/TrkA signaling *in vivo*. *Neuron* 25:345–357.
51. Lu J, Zhou XF, Rush RA (2001) Small primary sensory neurons innervating epidermis and viscera display differential phenotype in the adult rat. *Neurosci Res* 41:355–363.
52. Grynkiewicz G, Poenie M, Tsien RY (1985) A new generation of Ca^{2+} indicators with greatly improved fluorescence properties. *J Biol Chem* 260:3440–3450.
53. Caterina MJ, et al. (1997) The capsaicin receptor: A heat-activated ion channel in the pain pathway. *Nature* 389:816–824.
54. Lindsay RM (1996) Role of neurotrophins and trk receptors in the development and maintenance of sensory neurons: An overview. *Philos Trans R Soc Lond B Biol Sci* 351:365–373.
55. Terenzio M, et al. (2014) Bicaudal-D1 regulates the intracellular sorting and signalling of neurotrophin receptors. *EMBO J* 33:1582–1598.
56. Huang EJ, Reichardt LF (2003) Trk receptors: Roles in neuronal signal transduction. *Annu Rev Biochem* 72:609–642.
57. Patapoutian A, Reichardt LF (2001) Trk receptors: Mediators of neurotrophin action. *Curr Opin Neurobiol* 11:272–280.
58. Kitao Y, Robertson B, Kudo M, Grant G (1996) Neurogenesis of subpopulations of rat lumbar dorsal root ganglion neurons including neurons projecting to the dorsal column nuclei. *J Comp Neurol* 371:249–257.
59. Maro GS, et al. (2004) Neural crest boundary cap cells constitute a source of neuronal and glial cells of the PNS. *Nat Neurosci* 7:930–938.
60. Stucky CL, DeChiara T, Lindsay RM, Yancopoulos GD, Koltzenburg M (1998) Neurotrophin 4 is required for the survival of a subclass of hair follicle receptors. *J Neurosci* 18:7040–7046.
61. Smeyne RJ, et al. (1994) Severe sensory and sympathetic neuropathies in mice carrying a disrupted Trk/NGF receptor gene. *Nature* 368:246–249.
62. Ernfors P, Lee KF, Kucera J, Jaenisch R (1994) Lack of neurotrophin-3 leads to deficiencies in the peripheral nervous system and loss of limb proprioceptive afferents. *Cell* 77:503–512.
63. Moqrich A, et al. (2004) Expressing TrkC from the *TrkA* locus causes a subset of dorsal root ganglia neurons to switch fate. *Nat Neurosci* 7:812–818.
64. Fitzgerald M (2005) The development of nociceptive circuits. *Nat Rev Neurosci* 6:507–520.
65. von Hehn CA, Baron R, Woolf CJ (2012) Deconstructing the neuropathic pain phenotype to reveal neural mechanisms. *Neuron* 73:638–652.
66. Sleigh JN, Schiavo G (2016) Older but not slower: Aging does not alter axonal transport dynamics of signalling endosomes in vivo. *J Neurosci Methods* 257:26–33.
67. Sleigh JN, et al. (2014) Chondrolectin affects cell survival and neuronal outgrowth in *in vitro* and *in vivo* models of spinal muscular atrophy. *Hum Mol Genet* 23:855–869.
68. Sleigh JN, Weir GA, Schiavo G (2016) A simple, step-by-step dissection protocol for the rapid isolation of mouse dorsal root ganglia. *BMC Res Notes* 9:82.
69. Malin SA, Davis BM, Molliver DC (2007) Production of dissociated sensory neuron cultures and considerations for their use in studying neuronal function and plasticity. *Nat Protoc* 2:152–160.
70. Chaplan SR, Bach FW, Pogrel JW, Chung JM, Yaksh TL (1994) Quantitative assessment of tactile allodynia in the rat paw. *J Neurosci Methods* 53:55–63.
71. Carter RJ, Morton J, Dunnett SB (2001) Motor coordination and balance in rodents. *Curr Protoc Neurosci* Chapter 8:Unit 8.12.
72. Randall LO, Selitto JJ (1957) A method for measurement of analgesic activity on inflamed tissue. *Arch Int Pharmacodyn Ther* 111:409–419.
73. Hargreaves K, Dubner R, Brown F, Flores C, Joris J (1988) A new and sensitive method for measuring thermal nociception in cutaneous hyperalgesia. *Pain* 32:77–88.
74. Bogdanik LP, et al. (2013) Loss of the E3 ubiquitin ligase LRSAM1 sensitizes peripheral axons to degeneration in a mouse model of Charcot-Marie-Tooth disease. *Dis Model Mech* 6:780–792.